Earth Sciences
2026, Vol. 15, No. 2, pp. 109–124
https://doi.org/10.11648/j.earth.20261502.13

Research Article

Petrography and Geochemistry of Syenogranites and Gabbronorites from the Niergui Massif, Guéra Province, Chad

Guoldji Crepin Djamous[1], Tassongwa Bernard[1, *], Metang Victor[2], Ngassam-Mbianya Ghislain[1], Tamen Jules[1], Baïssemia Ronang Gustave[3], Jouanang Viclair Daina[2], Masonde Kouo Adelaïde Flore[1], Bikaga Clarisse Rosine[2], Nkoumbou Charles[2]

[1]Department of Earth Sciences, University of Dschang, Dschang, Cameroon
[2]Department of Earth Sciences, University of Yaoundé 1, Yaoundé, Cameroon
[3]Departement of Geological Engineering, University of Pala, Pala, Chad

Abstract

The Niergui Massif, located at the southern margin of the Sahara Metacraton, represents a poorly documented portion of the Pan-African basement in Chad. This study integrates petrographic and geochemical analyses of syenogranites and gabbronorites to better constrain their nature, origin, and the magmatic processes involved in basement formation. The syenogranites are strongly potassic calc-alkaline, weakly peraluminous, and ferroan, whereas the gabbronorites are metaluminous and moderately differentiated. Major, trace, and rare-earth element geochemistry indicates a progressive magmatic evolution: gabbronorites reflect a primitive mantle source, while syenogranites show enrichment in incompatible elements and differentiation toward crustal magmas. Sr/Y and Rb/Sr ratios, as well as Eu anomalies, suggest that syenogranites formed from a mixture of enriched mantle and crustal sources, whereas gabbronorites are weakly differentiated and mantle-derived. Nb/Zr vs. Zr diagrams and zircon saturation temperatures (700–850°C) indicate that magma crystallization involved both fractional crystallization and partial melting. Tectonic discrimination diagrams (Ta vs. Yb, Rb vs. Yb+Ta) confirm a subduction setting followed by a syn- to post-collisional phase, consistent with the Pan-African dynamics between the Congo Craton and the Adamawa-Yadé block. These results indicate that the Niergui Massif exemplifies a bimodal magmatic system, characterized by mantle–crust interaction, partial melting, and fractional crystallization. The complexity of geochemical signatures reflects local variations and multiple stages of magmatic evolution from mantle to differentiated crustal magmas. This study provides a solid framework for understanding Pan-African geodynamics in the Guéra region and contributes to the characterization of the Neoproterozoic basement of the Sahara Metacraton.

Keywords

Syenogranites, Gabbronorites, Bimodal Magmatism, Subduction, Guéra, Pan-African

*Correspondence: Tassongwa Bernard (bernard.tassongwa@univ-dschang.org), Tassongwa Bernard (btassongwa2004@gmail.com)

Received: 26 February 2026; **Accepted:** 16 March 2026; **Published:** 23 April 2026

1. Introduction

Located at the southern margin of the Sahara Metacraton, the central Chadian massif of Guéra is poorly documented due to the scarcity of outcrops. It is composed of metamorphic and magmatic rocks associated with the collision between the Congo–São Francisco Craton and the Sahara Metacraton. The Neoproterozoic Guéra basement is dominated by granitoids and mafic enclaves [16, 17, 23, 25, 41]. Several studies suggest that these rocks result from mixing between mantle-derived and crustal magmas, reflecting the complexity of the geodynamic processes involved [11, 16, 21]. Further south, in the Melfi Massif, syenites and granites enriched in alkalis and light rare earth elements, associated with positive Eu anomalies, indicate the involvement of partial melting of garnet-amphibolite sources with a contribution from metasomatized mantle [4]. Magmatic activity in this region lasted for approximately 50 Ma, from 595 to 545 Ma [44, 45], while U–Th–Pb zircon ages ranging from 1.9 Ga to 580 Ma document Pan-African crustal recycling. The oldest granites (595 ± 8 Ma and 589 ± 6 Ma) are metaluminous to peraluminous, magnesian, with alkaline to calc-alkaline signatures, whereas the younger granites (≤ 570 Ma) are peraluminous, ferriferous, alkali-calcic, and post-collisional [4, 44]. Two generations of post-collisional granites are distinguished: first, arc-type hornblende–biotite granites (~595 Ma) derived from partial melting of subduction-modified mantle; second, biotite granites (~590 Ma) emplaced during crustal relaxation following an oblique collision [18, 41]. A second post-collisional magmatic phase, after crustal thinning, eventually produced granites around 560 Ma [18, 41]. Despite these advances, the central Chadian massif remains largely unexplored, and the nature, origin, and evolution of the Guéra formations remain key questions. This knowledge gap limits the understanding of Pan-African dynamics in this portion of the orogen. The present study aims to address this gap by characterizing the formations of Niergui and its surroundings through a petrographic and geochemical approach, in order to constrain their origin and improve understanding of the magmatic processes involved in the construction of the Pan-African Chadian basement.

2. Geological Setting

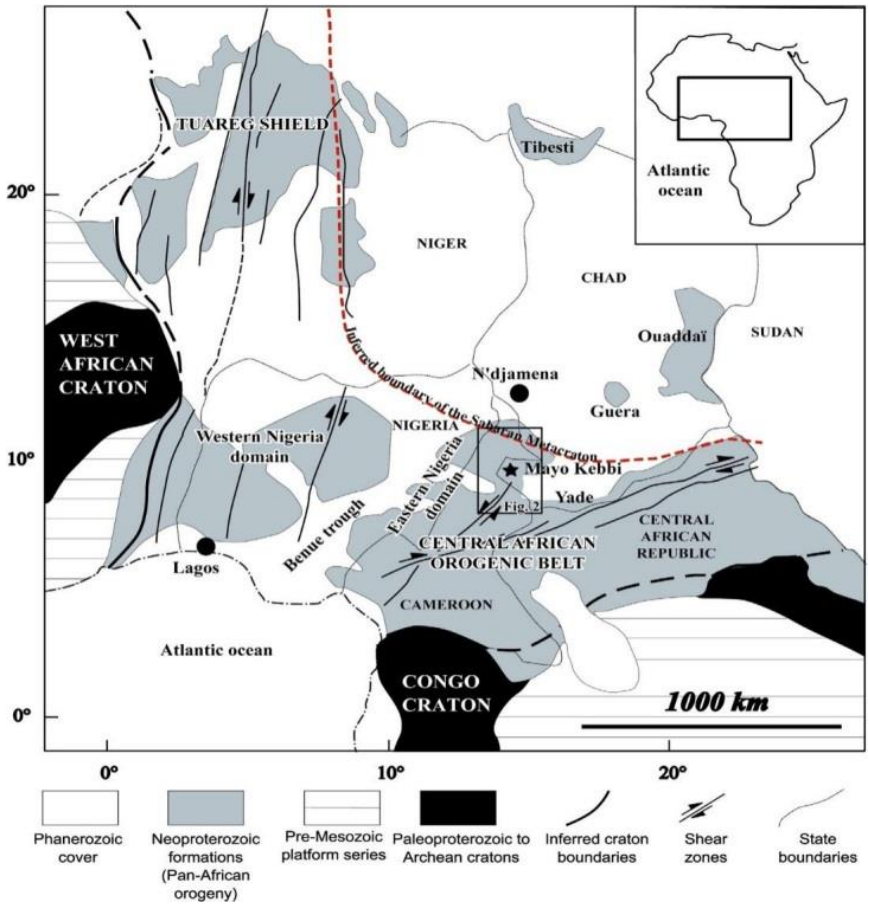

Figure 1. *Location of the study area within the geological framework of North-Central Africa (modified after [52, 24]. The inferred boundary of the Saharan Metacraton is drawn after Abdelsalam et al. [1].*

The Pan-African orogeny, initially interpreted as a simple reactivation of Archean structures [26], is now widely recognized as a major Neoproterozoic thermo-tectonic event that profoundly shaped Gondwana between ~700 and 500 Ma, with a peak of activity around 600 ± 100 Ma [6, 53]. In Central Africa, this orogeny is notably expressed by the development of the Oubanguides belt, characterized by large sublatitudinal (E–W) shear zones and high-grade metamorphism [35, 41]. In Chad, the Precambrian basement inherited from this orogeny lies within a complex junction zone between the Congo Craton, the Eastern Nigerian domain, and the Saharan Metacraton [23, 24]. The Chadian Central Massif, including the Guéra, Kenga, and Melfi massifs, occupies a strategic geodynamic position between the Chad Craton, the Darfur block, and the Congo Craton (Figure 1). This setting makes it a key domain for investigating crustal evolution and crust–mantle interactions during the Pan-African orogeny [2, 30]. The earliest geological descriptions of the Chadian Central Massif date back to the works of Freydenberg [19] and Lacroix [27], later complemented by the detailed studies of Vincent [54]. These authors highlighted the existence of three successive major magmatic cycles, referred to as gA, gB, and gC, as well as the occurrence of so-called malgachitic facies, showing affinities with the charnockites of southern India. Subsequent studies also documented a variety of metamorphic rocks, including quartzites, micaschists, gneisses, and tactites, generally occurring as enclaves within granitoid plutons [55, 59].

Lithologically, the Chadian Central Massif is dominated by intense Pan-African magmatism, mainly represented by granitoids (granodiorites, granites, and charnockites), associated with intermediate to mafic rocks such as diorites and gabbros [2, 23]. These magmatic formations account for nearly 90% of the crustal edifice of the massif. Three main lithological units are classically distinguished: (1) the younger granites, of Pan-African to post-Pan-African age, generally forming prominent reliefs and locally occurring as inselbergs; (2) a heterogeneous granitic complex, predominantly calc-alkaline in composition, widely distributed throughout the massif and commonly characterized by abundant enclaves of older rocks; and (3) the older granodioritic series, occurring as bands and enclaves, comprising granodiorites, diorites, and locally gabbros, and displaying charnockitic affinities comparable to the malgachitic series described by Lacroix [27]. Finally, this assemblage is crosscut by late mafic intrusions, represented by small gabbroic bodies and doleritic to microgabbroic dykes, attesting to magmatic activity subsequent to the emplacement of the main Pan-African granitoids [36, 54].

3. Methodology

The present study is based on an integrated methodological approach combining field observations, petrographic analyses, and geochemical investigations in order to characterize the nature, composition, and geological evolution of the study area. Fieldwork involved direct observations of outcrops, including macroscopic descriptions of lithologies, structural mapping, and the collection of representative rock samples. These observations allowed refinement of the lithological typology, spatial distribution, and contact relationships between the different rock units. Petrographic investigations were carried out on thin sections prepared according to standard procedures at the Institute of Geological and Mining Research (IRGM), Yaoundé. Microscopic observations were conducted under polarized light to identify mineral assemblages, textures, and microstructures characteristic of the studied rocks. For geochemical analyses, each sample was crushed and homogenized. Approximately 25 g of powder, with an average grain size of ~75 µm, were collected, packaged in appropriate containers, and sent to ACTLABS laboratories (Ontario, Canada) and ALS Geochemistry (Johannesburg, South Africa). Major elements and selected trace elements were analyzed by inductively coupled plasma–optical emission spectrometry (ICP-OES), whereas trace elements and rare earth elements were determined by inductively coupled plasma–mass spectrometry (ICP-MS). In total, twenty-four (24) rock samples (labelled ENGxx) were collected during this study (Figure 8). Of these, thirteen (13) samples were selected for thin-section preparation, and five (5) representative samples were retained for whole-rock geochemical analyses.

4. Results

4.1. Petrography

Petrographic results indicate that the study area is mainly composed of plutonic rocks, which can be grouped into two major lithological domains: a granitoid domain and a gabbroic domain (Figure 2). The granitoid domain comprises syenogranites, amphibole–biotite monzogranites, biotite monzogranites, quartz–alkali feldspar syenites, and quartz syenites. The gabbroic domain is exclusively represented by gabbronorite.

4.1.1. Field Observations

Granitoids mainly crop out as metric to plurimetric blocks, producing a chaotic landscape typical of granitic boulder fields. Locally, these rocks occur as exposed slabs (Figure 3a). In outcrop, they are generally light grey in colour and display medium- to coarse-grained textures. Amphibole–biotite monzogranite is locally crosscut by discordant veins (Figure 3b). These veins, centimetric in thickness, are characterized by a pinkish-grey colour, metric to plurimetric continuity and fine- to medium-grained textures. Their relatively homogeneous internal structure, combined with their crosscutting geometry and finer grain size compared to the host rock, suggests a late-stage emplacement. Quartz–alkali feldspar syenites crop

out as blocks ranging from 0.5 to 8 m in size. They are distinguished by the presence of orthoclase phenocrysts, a pinkish-grey colour, and a dark weathering patina. Gabbronorite occurs mainly as enclaves within the granitic bodies, particularly within syenogranites (Figure 4b). These enclaves display characteristic sigmoidal morphologies, with sizes ranging from centimetric to metric. In addition, metric to plurimetric gabbronorite blocks were also observed (Figure 4a), indicating heterogeneity in emplacement modes. The rock is dark grey to black in colour, with fine- to medium-grained textures reflecting its high mafic mineral content.

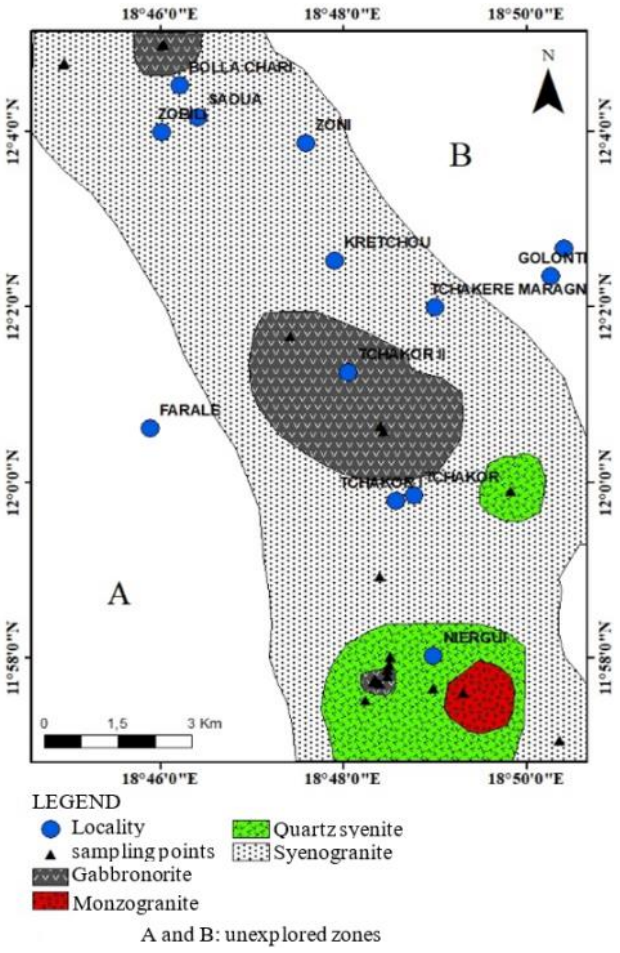

Figure 2. *Geological map of the study area.*

4.1.2. Microscopic Observations

Under the microscope, granitoids display a porphyroid granular texture (Figure 3d). Their mineral assemblage is dominated by alkali feldspar, quartz, plagioclase, biotite, and amphibole. Accessory minerals include opaque phases, zircon, apatite, sphene (titanite), and locally chlorite. Alkali feldspars are generally rectangular to sub-rectangular in shape and are represented by orthoclase and microcline, with orthoclase being predominant. Some orthoclase crystals show microfractures filled with quartz, perthitic textures, and locally Carlsbad twinning (Figure 3c). Microcline commonly exhibits sericitization. Quartz is generally polycrystalline (Figure 3d) and occurs in two main forms: (i) small subgrains, commonly included within feldspars or located along their margins, and (ii) quartz ribbons with undulose extinction, reaching up to 0.4 mm in length and 0.2 mm in width, indicative of intracrystalline deformation. Plagioclase occurs as euhedral to subhedral crystals, commonly twinned, with mechanical twins arranged in wedge- or spindle-shaped patterns. Some crystals contain quartz inclusions. Biotite occurs as elongated crystals (Figure 3e) or as xenomorphic grains with irregular outlines (Figure 3d). It locally contains inclusions of opaque minerals and zircon and shows partial alteration to chlorite (Figure 3e). In some cases, biotite molds alkali feldspar crystals (Figure 3c). Amphiboles are generally subhedral. Some crystals contain inclusions of opaque minerals, whereas others display partial destabilization to chlorite, reflecting late-stage alteration or re-equilibration processes. All samples belonging to the gabbroic domain are gabbronoritic in nature and are more precisely classified as clinopyroxene-bearing norites according to the P–Opx–Cpx (Plagioclase-Orthopyroxene-Clinopyroxene) diagram of Streckeisen [46]. They are characterized by granular to doleritic textures, typically intergranular (Figure 4f). The mineral assemblage is dominated by plagioclase, orthopyroxene, and clinopyroxene, associated with biotite, orthoclase, amphibole, and opaque minerals. A notable difference is observed among samples: some (ENG6 and ENG25) contain interstitial xenomorphic quartz located along the margins of major crystals, whereas others (ENG9 and ENG19) lack any quartz phase.

Plagioclase crystals occur as elongated laths, reaching up to 1.6 mm in length and approximately 0.5 mm in width (Figure 4f). These crystals are commonly intergrown, imparting a texture characteristic of relatively rapid cooling. Interstices between plagioclase crystals are generally occupied by amphiboles and opaque minerals (Figure 3d). Some plagioclase crystals contain inclusions of pyroxene and opaque minerals (Figure 4e) and locally show sericitic alteration. Mechanical twins, in the form of spindle- or wedge-shaped patterns, are also observed (Figure 4f). Pyroxenes in the gabbronorite are predominantly xenomorphic. Orthopyroxene (Opx) is the dominant pyroxene, whereas clinopyroxene (Cpx) occurs in lower proportions, generally occupying interstitial spaces between plagioclase crystals and in proximity to orthopyroxene grains.

4.2. Geochemistry

In order to characterize the main geochemical properties, five representative whole-rock samples were analyzed (Tab. 1): two syenogranites (ENG10 and ENG16) and three gabbronorites (ENG9, ENG19, and ENG25). The results were interpreted using typological binary diagrams and geochemical discrimination plots, allowing a better assessment of the nature and origin of the studied units.

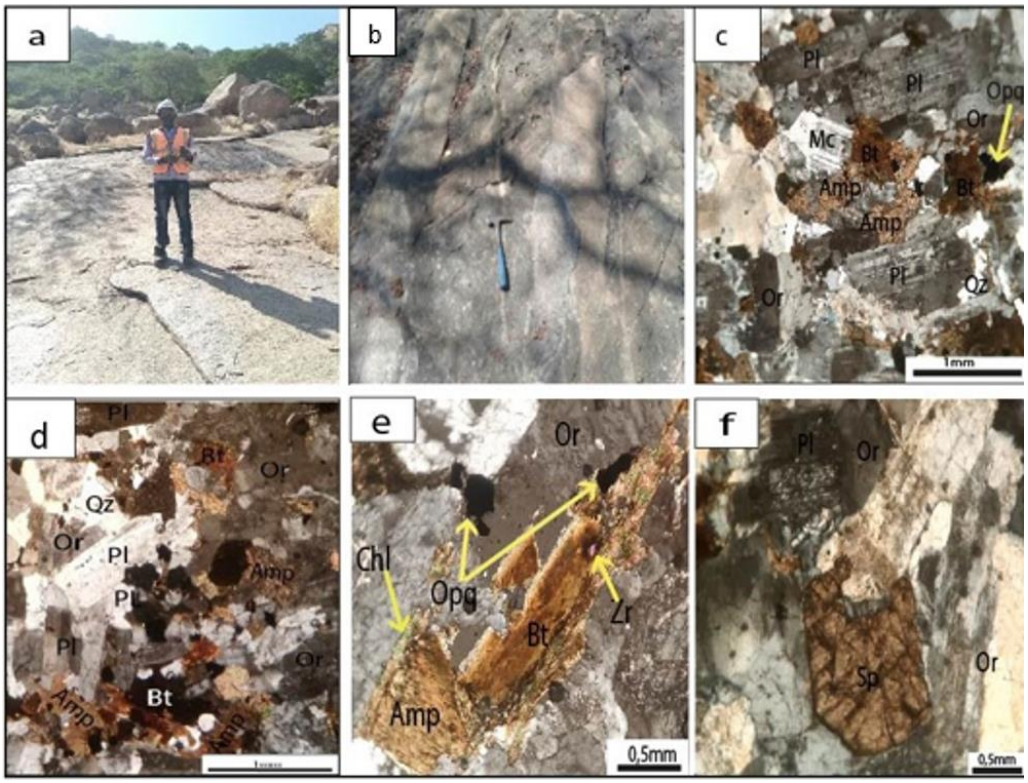

Figure 3. *Field photographs and photomicrographs of granitoids: (a) Slab outcrop and block of syenogranite at Niergui; (b) Slab outcrop of amphibole–biotite monzogranite crosscut by a greyish-pink dyke; (c) Photomicrograph showing a coarse-grained porphyritic texture; (d) Thin-section view highlighting perthitic structure and microfractures; (e) Photomicrograph showing a zircon crystal included in biotite and biotite destabilization into chlorite; (f) Thin-section view highlighting sphene (titanite) crystals adjacent to alkali feldspars.*

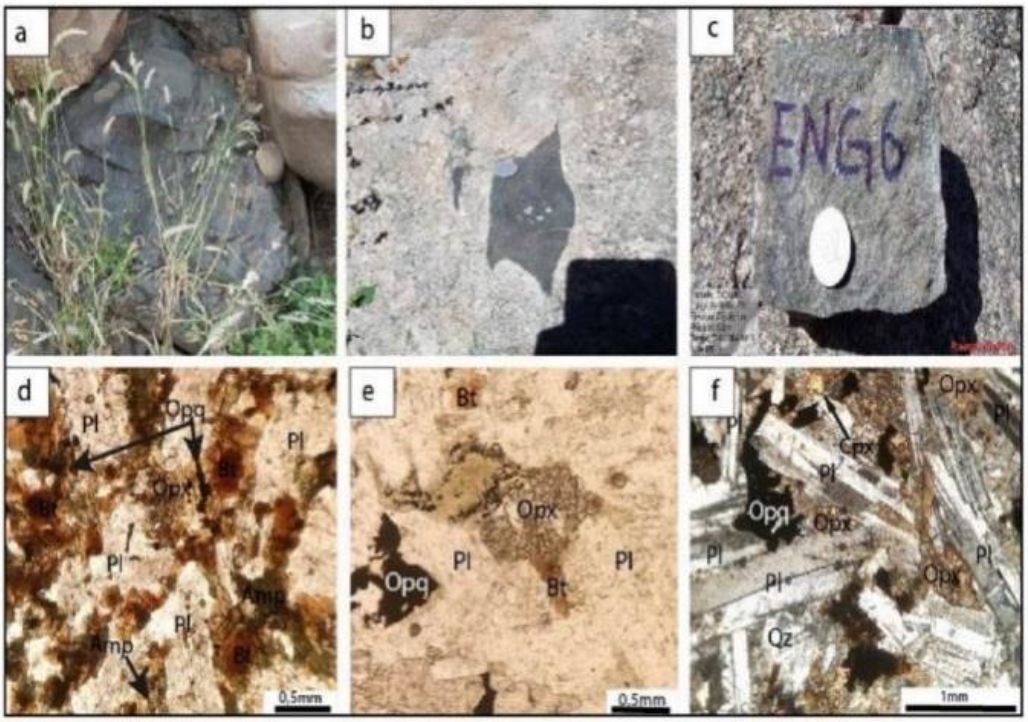

Figure 4. *Field photographs and photomicrographs of gabbronorite: (a) Block outcrop; (b) Gabbronorite enclave within the surrounding granites; (c) Hand sample of gabbronorite; (d) Opaque minerals and biotite inclusions within plagioclase; (e) Thin-section view highlighting inclusions of pyroxene and opaque minerals within plagioclase; (f) Photomicrograph showing a coarse-grained to intergranular doleritic texture.*

4.2.1. Major Elements

Table 1 presents whole rocks major eements content and normative composition. The syenogranites are characterized by high SiO_2 (69.00–70.00 wt%) and Al_2O_3 (14.40–15.25 wt%) contents. K_2O (4.78–5.43 wt%) and Na_2O (3.33–3.81 wt%) concentrations are also high, whereas Fe_2O_3 (2.42–3.05 wt%), MnO (0.04 wt%), P_2O_5 (0.10–0.22 wt%), TiO_2 (0.34–0.39 wt%), MgO (0.50–0.73 wt%), and CaO (1.78–1.88 wt%) remain low. The K_2O/Na_2O ratio ranges from 1.43 to 1.44, indicating a strongly potassic composition.

Gabbronorites display moderate SiO_2 (47.30–51.00 wt%) and Al_2O_3 (14.35–14.95 wt%) contents, and high concentrations of Fe_2O_3 (13.40–13.60 wt%), CaO (6.77–7.77 wt%), MgO (3.90–6.22 wt%), TiO_2 (2.34–2.88 wt%), MnO (0.17–0.18 wt%), and P_2O_5 (0.78–1.26 wt%), whereas K_2O (1.35–2.18 wt%) and Na_2O (2.85–2.92 wt%) are relatively low. CIPW normative calculations for the syenogranites yield the following proportions: quartz 21.85–26.11%, orthoclase 28.95–32.26%, albite 28.88–32.41%, anorthite 8.23–8.29%, and hypersthene 3.50–4.80%. Accessory normative phases include magnetite (0.08–0.82%), ilmenite (0.65–0.76%), and apatite (0.22–0.49%). Normative corundum is present in very low amounts (0.77%). The very high differentiation index (DI = 83.93–86.51%) highlights the advanced magmatic evolution of the syenogranites. In the gabbronorites, normative corundum is absent, indicating a clearly metaluminous signature. Sample ENG9 lacks normative quartz but contains a considerable amount of normative olivine (5.40%), suggesting a slightly more basic composition. Normative proportions reveal a dominance of pyroxenes, with diopside ranging from 5.63 to 9.36% and hypersthene from 20.04 to 21.21%. Feldspars are represented by orthoclase (8.55–13.19%), albite (25.12–25.86%), and anorthite (20.08–25.31%), with normative quartz amount of 1.22 and 3.80% for ENG19 and ENG25 respectively. Accessory phases include ilmenite (4.55–5.60%), magnetite (2.37–2.51%), and apatite (1.83–2.82%). The moderate differentiation index (DI = 34.32–42.29%) indicates that the gabbronorites are moderately differentiated.

(i). Rock Classification

The multicational R1–R2 diagram [12, 14] classifies the granitic rocks as monzogranites, whereas the gabbroic rocks plot within the gabbrodiorite field (Figure 5a). The Q′–ANOR diagram [47] confirms the syenogranitic, monzogranitic, and gabbroic classifications for the respective samples (Figure 5b).

(ii). Magmatic Affinity

In the TAS diagram [28], syenogranites and gabbronorites plot within the acidic and basic fields, respectively (Figure 6a). Their position below the dividing line of Irvine and Baragar [22] indicates affiliation with the subalkaline series. Complementary analysis using the AFM diagram [22] shows that all samples belong to the calc-alkaline series (Figure 6b).

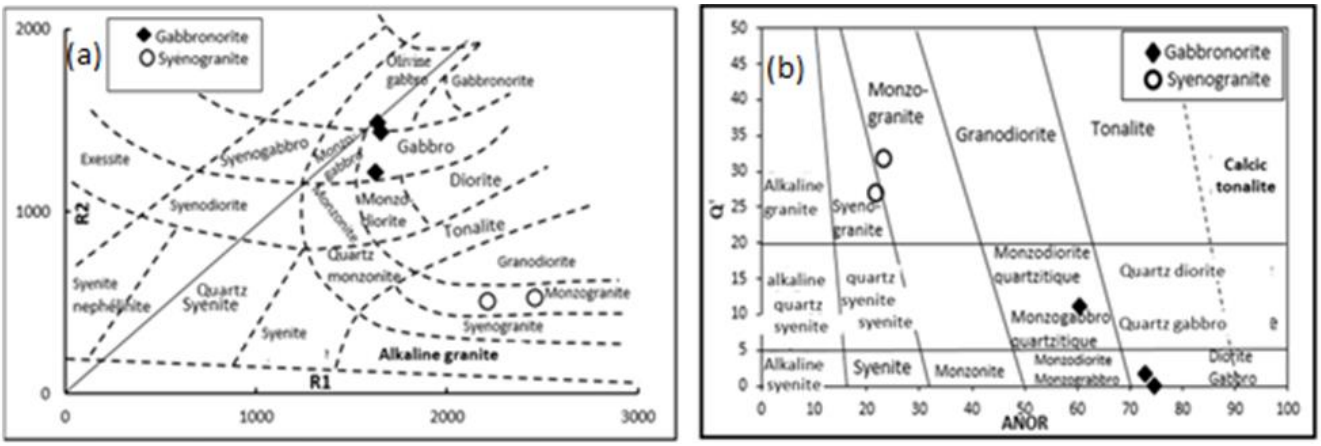

Figure 5. Classification of Niergui studied rocks. (a) R1–R2 cationic diagram of De La Roche et al. [12], where R1 = 4Si − 11(Na + K) − 2(Fe + Ti) and R2 = 6Ca + 2Mg + Al; (b) Normative Q'–ANOR diagram of Streckeisen and Le Maitre [47], where ANOR = 100 × An/(An + Or) and Q' = 100 × Q/(Q + Or + Ab + An).

This classification is further supported by the K_2O vs. SiO_2 diagram of Le Maitre et al. [29], which highlights the overall calc-alkaline affinity of the rocks (Figure 6c). More specifically, the syenogranites display a strongly potassic calc-alkaline signature evolving toward the shoshonitic field, whereas the gabbronorites exhibit moderate to slightly elevated potassium contents. Finally, the $FeO_t/(FeO_t + MgO)$ diagram [20] indicates that the syenogranites plot within the ferroan field, whereas the gabbronorites are magnesian to slightly ferroan, close to the boundary between these two domains (Figure 6d).

In the A–B cationic diagram [13], the syenogranites fall within field III, characteristic of peraluminous rocks, whereas the gabbronorites occupy field IV, corresponding to metaluminous rocks (Figure 7a). The A/NK vs. A/CNK diagram

([31]; Figure 7b) confirms this distinction. The syenogranites are weakly peraluminous, plotting close to the boundary with the metaluminous domain, and are assigned to I-type granites. The gabbronorites plot clearly within the metaluminous field, indicating low alumina saturation consistent with an I-type affinity.

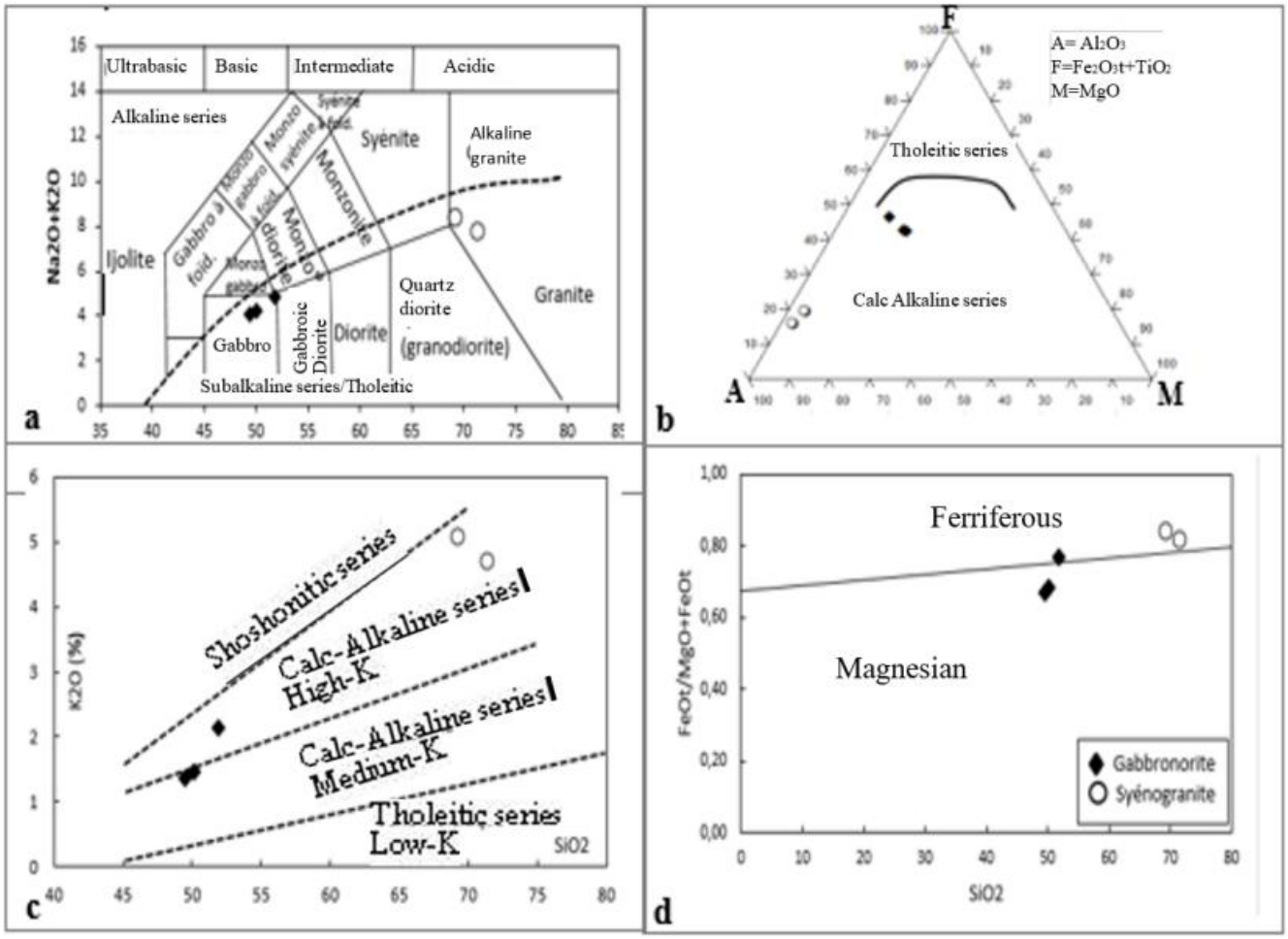

Figure 6. *Magmatic affinities of the studied rocks: (a) $Na_2O + K_2O$ vs. SiO_2 diagram [29]; (b) AFM diagram [22]; (c) K_2O vs. SiO_2 diagram [22]; (d) FeO/(MgO + FeO) vs. SiO_2 diagram [20].*

Table 1. *Whole rock major elements, normative composition and selected ratios.*

Rock type	**Syenogranite**		**Gabbronorite**		
Sample	**ENG16**	**ENG10**	**ENG25**	**ENG9**	**ENG19**
SiO2	70.00	69.00	51.00	48.80	47.30
TiO_2	0.34	0.39	2.88	2.34	2.35
Al_2O_3	15.25	14.40	14.35	14.95	14.8
Fe_2O_3t	2.42	3.05	13.4	13.55	13.6
MnO	0.04	0.04	0.17	0.18	0.18
MgO	0.50	0.73	3.90	6.22	3.48
CaO	1.78	1.88	6.77	7.53	7.77
Na_2O	3.81	3.33	2.92	2.90	2.85

Rock type	Syenogranite		Gabbronorite		
Sample	ENG16	ENG10	ENG25	ENG9	ENG19
K_2O	5.43	4.78	2.18	1.52	1.35
P_2O_5	0.10	0.22	1.26	0.89	0.78
LOI	0.67	0.87	0.70	1.07	0.39
Total	100.34	98.69	99.53	99.95	94.85
A/CNK	1.38	1.44	1.21	1.25	1.24
A/NK	1.65	1.78	2.81	3.38	3.52
K_2O/Na_2O	1.43	1.44	0.75	0.52	0.47
K_2O+Na_2O	9.24	8.11	5.10	4.42	4.20
CaO/Na_2O	0.47	0.56	2.32	2.60	2.73
Al_2O_3/TiO_2	44.85	36.92	4.98	6.39	6.30
Mg*	34	38	40	51	37
Normative composition					
Quartz	21.85	26.11	3.80	-	1.22
Orthose	32.26	28.95	13.19	9.20	8.55
Albite	32.41	28.88	25.30	25.12	25.86
Anorthite	8.29	8.23	20.08	23.84	25.31
Diopside	-	-	5.63	7.47	9.36
Hypersthène	3.50	4.80	21.21	20.04	20.57
Olivine	-	-	-	5.40	-
Magnétite	0.75	0.96	2.37	2.39	2.51
Ilménite	0.65	0.76	5.60	4.55	4.79
Corindon	0.08	0.82	-	-	-
Apatite	0.22	0.49	2.82	1.99	1.83
TOTAL	100.00	100.00	100.00	100.00	100.00
DI	86.51	83.93	42.29	34.32	35.64

4.2.2. Trace Elements and Rare Earth Elements

The syenogranites are characterized by very high Ba (1440–1995 ppm) and Rb (149.4–180 ppm) contents (Tab. 2), reflecting strong enrichment in elements compatible with K-feldspar. Sr (548–825 ppm) and Zr (182–206 ppm) contents are moderate to relatively high, whereas Sc (1.9–3.9 ppm), Cr (12–13 ppm), Y (10.8–20.3 ppm), and V (24–37 ppm) contents remain low. Gabbronorites also display high Ba contents (796–1216 ppm), slightly lower than those of the syenogranites, but very low Rb contents (32.3–60.2 ppm). Sr (523–596 ppm) and Zr (241–513 ppm) are moderate, whereas Cr (65–177 ppm), V (195–209 ppm), Sc (27–28.4 ppm), and Y (34.1–56.9 ppm) are obviously higher than in the syenogranites, indicating a more primitive signature enriched in elements associated with mafic minerals. Primitive mantle–normalized multi-element diagrams [32] show distinct trends for the two rock types. Syenogranites (Figure 8a) display negatively sloping patterns, indicating enrichment in large-ion lithophile elements (LILE) relative to high-field-strength elements (HFSE), with pronounced peaks and troughs. Positive anomalies are observed for Ba, U, K, Sr, Zr, Hf, Ti and Tm, whereas negative anomalies occur for Th, Nb, Pr, Nd and Er. Gabbronorites (Figure 8a) also show negative slopes, but with overall higher concentrations than those of the syenogranites. They are characterized by positive anomalies in Cs, Ba, K, La, Nd, Sm, Ti, and Tm, and negative anomalies in Rb, Th, and Sr. Overall, both rock

groups are enriched in incompatible elements; however, syenogranites display lower abundances and more irregular patterns, suggesting significant magmatic fractionation and differentiation processes. Total rare earth element contents (ΣREE) in the syenogranites range from 40.95 to 171.59 ppm. Chondrite-normalized REE patterns [32] indicate enrichment in light rare earth elements (LREE) relative to heavy rare earth elements (HREE), with $(La/Yb)_n$ ratios of 2.94–25.22. Syenogranites show no significant europium anomaly, with Eu/Eu* values ranging from 0.92 to 1.06 (Figure 8b).

Gabbronorites exhibit higher and more variable ΣREE contents (209.58–431.49 ppm). Their REE patterns are also characterized by LREE enrichment relative to HREE, with $(La/Yb)_n$ ratios of 8.68–10.03, and display a slight negative Eu anomaly (Eu/Eu* = 0.73–0.92) (Figure 8b). Overall, syenogranites and gabbronorites share broadly similar geochemical patterns, although gabbronorites are richer in trace elements and REE, reflecting a less differentiated and more primitive magmatic character.

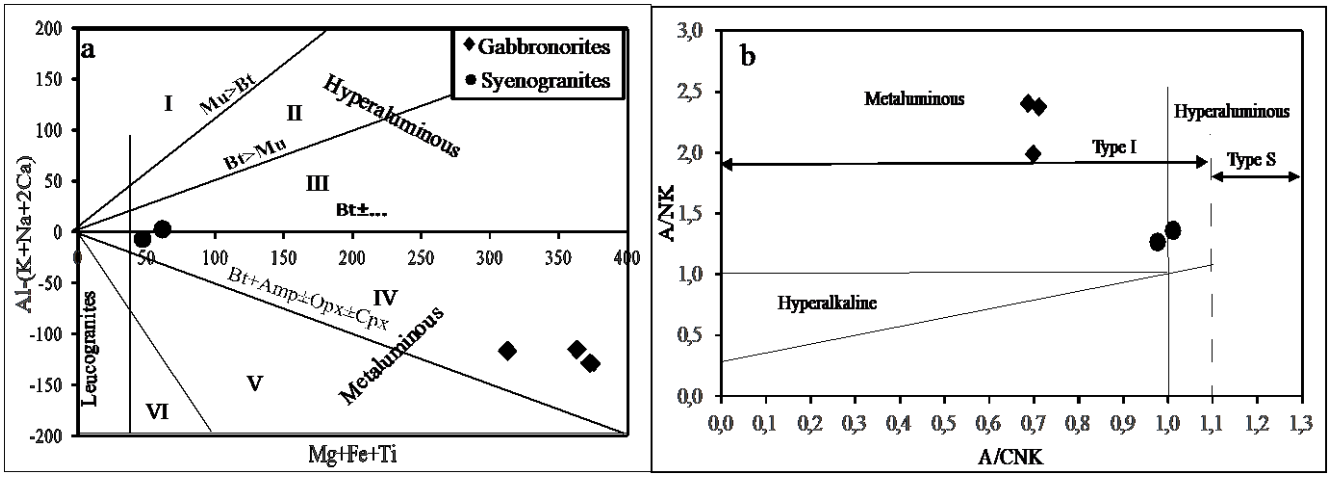

Figure 7. Metaluminous and peraluminous character of the rocks: (a) A–B cationic diagram illustrating the alumina balance [13], where A = Al − (K + Na + 2Ca) and B = Mg + Fe + Ti; (b) Maniar and Piccoli [31] diagram showing A/NK = $Al_2O_3/(Na_2O + K_2O)$ versus A/CNK = $Al_2O_3/(CaO + Na_2O + K_2O)$.

Table 2. Trace elements and selected ratios.

Rock type	Syenogranite		Gabbronorite		
Sample	ENG16	ENG10	ENG25	ENG9	ENG19
Ba	1995	1440	1300	861	780
Cr	12	13	65	176	177
Rb	180	149.5	60.2	39.1	32.3
Sr	825	548	596	529	523
V	24	37	204	195	209
Y	10.80	20.30	56.90	37.70	34.10
Zr	206	182	513	272	241
Hf	5.07	5.03	11.35	6.43	5.93
Ta	0.60	0.80	1.50	1.10	0.90
W	0.70	1.00	1.30	0.90	0.90
Th	6.91	0.74	4.96	3.45	2.8
U	1.54	1.08	0.84	0.70	0.61
Nb	7.69	7.41	30.50	18.00	16.10

Rock type	Syenogranite		Gabbronorite		
Sample	ENG16	ENG10	ENG25	ENG9	ENG19
Cs	2.18	2.09	1.61	0.95	0.50
Ga	21.9	22.8	24.9	22.9	22.0
Sn	2.5	5.1	3.3	2.7	2.1
Sc	1.9	3.9	27.3	27	28.4
La	40.4	6.8	77.7	42.8	35.2
Ce	76.7	16.0	172.0	95.0	78.9
Pr	8.63	2.02	22.40	12.50	10.40
Nd	31.6	9.3	94.6	55.4	47.3
Sm	4.56	2.55	17.9	10.35	9.17
Eu	1.30	0.96	4.10	3.09	2.77
Gd	3.28	3.02	15.85	10.45	9.04
Tb	0.38	0.54	2.07	1.34	1.23
Dy	1.98	3.69	11.4	6.97	6.97
Ho	0.35	0.78	2.10	1.45	1.22
Er	0.93	2.1	5.57	3.92	3.53
Tm	0.16	0.29	0.76	0.50	0.47
Yb	1.15	1.66	4.30	3.06	2.91
Lu	0.17	0.24	0.74	0.48	0.47
Sr/Y	76.40	27.00	10.48	14.03	15.34
Nb/Ta	12.82	9.26	20.33	16.36	17.89
Th/Yb	6.01	0.45	1.15	1.13	0.96
Zr/Hf	40.63	36.18	45.20	42.30	40.64
Nb/Zr	0.037	0.04	0.06	0.07	0.07

5. Discussion

5.1. Nature

According to Barbarin [5], granitoids can be classified into seven types based on their mineralogical assemblages, petrographic and field characteristics, as well as their chemical and isotopic signatures: MPG (muscovite-bearing peraluminous granitoids), CPG (cordierite-bearing peraluminous granitoids), KCG (K-rich calc-alkaline granitoids), ACG (amphibole-rich calc-alkaline granitoids), RTG (ridge tholeiitic granitoids), ATG (arc tholeiitic granitoids), and PAG (peralkaline and alkaline granitoids). The K_2O vs. SiO_2 diagram of Le Maitre et al. ([29]; Figure 6c) indicates that the Niergui syenogranites are strongly potassic calc-alkaline rocks. According to this classification, they therefore belong to the KCG type. These rocks are also weakly peraluminous and ferroan [4].

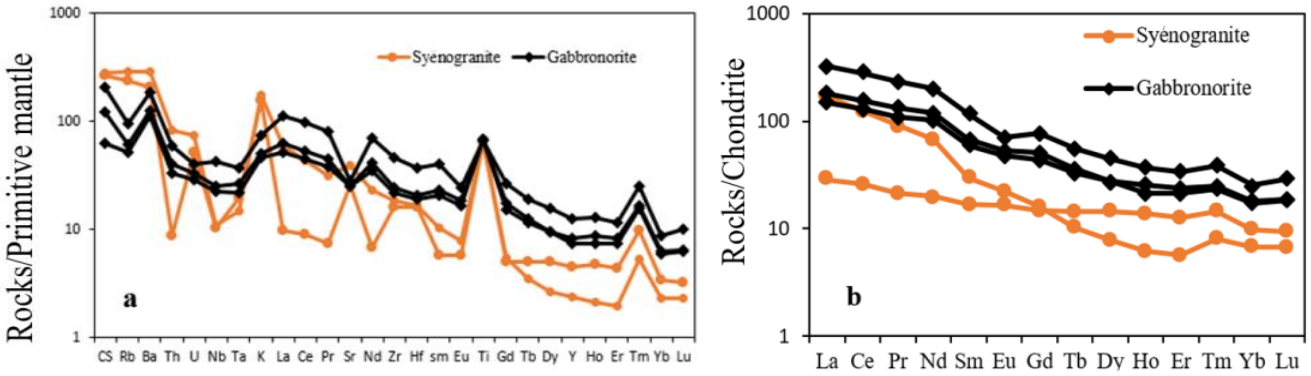

Figure 8. *Normallisation diagrams: (a) Primitive mantle-normalized trace element spider diagrams (normalization values from [32]; (b) Chondrite-normalized rare earth element (REE) patterns [32].*

The Niergui gabbronorites display a calc-alkaline signature with moderate to slightly elevated potassium contents and a metaluminous character, linking them to I-type granitoids. Their relatively low $FeO_t/(FeO_t + MgO)$ ratios, as defined by the diagram of Frost et al. [20] ($FeO_t/(FeO_t + MgO) = 0.67–0.77$), indicate a magnesian composition, comparable to that of ACG-type granitoids. This interpretation is supported by the work of Diontar et al. [16] on the Bitkine gabbro-diorites from the Guéra Massif, which exhibit similar geochemical characteristics. The relatively high Sr (>300 ppm) and Ba (>500 ppm) contents, combined with low Rb concentrations, suggest that these rocks correspond to "high-Sr granitoids" according to the classification of Tarney and Jones [48]. Finally, the Sr/Y vs. Y diagram (Figure 9) shows that most samples correspond to typical calc-alkaline rocks. However, one syenogranite sample is distinguished by a Sr/Y ratio greater than 40, indicating an adakitic affinity [15].

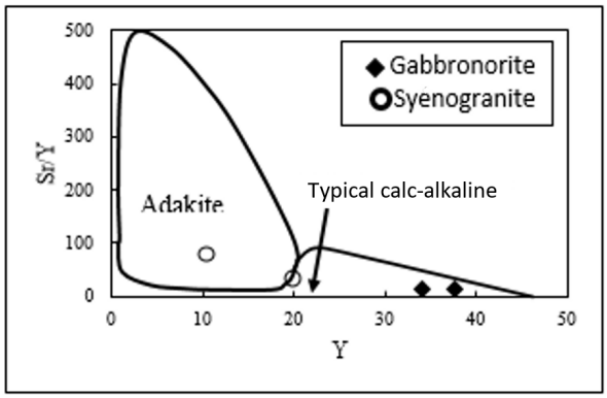

Figure 9. *Sr/Y vs. Y discrimination diagram [15].*

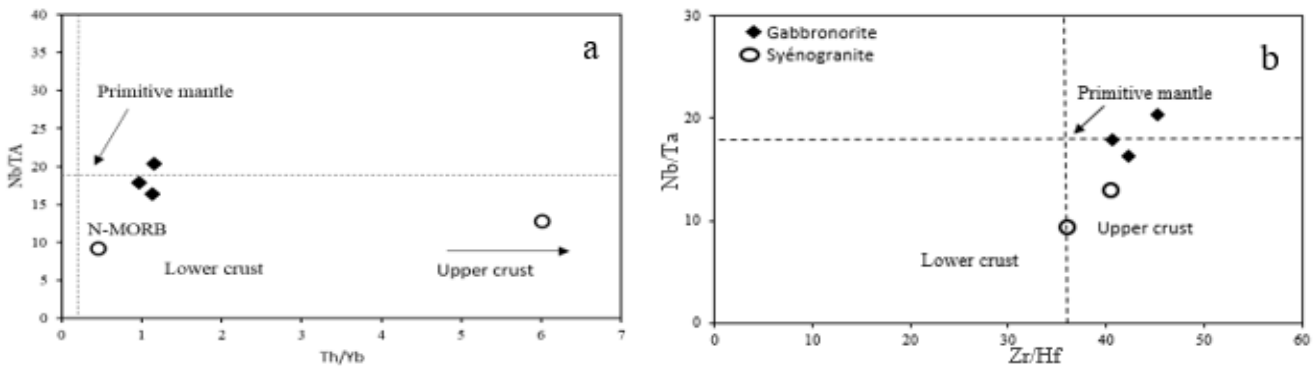

Figure 10. *Source characteristics of the Niergui formations and surrounding rocks: (a) Nb/Ta vs. Th/Yb diagram; (b) Nb/Ta vs. Zr/Hf diagram. N-MORB, OIB, and primitive mantle values are from McDonough and Sun [32], whereas upper and lower continental crust values are from Wedepohl [57].*

5.2. Magma Source

The syenogranites from the study area display calc-alkaline, high-K to shoshonitic, ferroan, and weakly peraluminous characteristics. Their petrographic and geochemical compositions meet the criteria of I-type granitoids as defined by Barbarin [5], suggesting a petrogenesis from a mixed magma source involving both mantle and crustal contributions. Geochemical analysis of the syenogranites and gabbronorites reveals several significant trends. Most samples exhibit Sr/Y ratios ranging from 10.47 to 27, consistent with classical calc-alkaline arc or active-margin magmatism associated with partial melting or differentiation processes [10, 42]. However, one isolated syenogranite sample is distinguished by a high Sr/Y ratio (76.39) and Sr contents exceeding 500 ppm, indicative of adakitic behavior [9, 15]. This signature may result either from derivation from a deep or thickened crustal source, or from specific internal magmatic processes such as the accumulation of Sr-rich phases or relative Y depletion during fractional crystallization [7]. Ba/Sr ratios ranging from 1.49 to 2.63 suggest moderate crustal contamination, consistent with magma interaction with Ba-enriched felsic sources, while the least differentiated magmas retain a mantle-derived component [51]. The syenogranites also show relatively high Rb/Sr ratios (0.22–0.27), typical of crustal-derived rubidium enrichment [49], whereas the gabbronorites display lower values (0.06–0.10), compatible with a weakly differentiated mantle magma [43]. Nb/Ta vs. Th/Yb and Nb/Ta vs. Zr/Hf diagrams (Figure 10) indicate a progressive magmatic evolution from gabbronorites toward syenogranites, reflecting a transition from a mantle source (primitive mantle or N-MORB-like) toward a crustal signature. This evolution suggests a bimodal system marked by strong mantle–crust interaction, as documented in other Pan-African complexes of Chad [16, 44, 45]. The most likely source is an enriched mantle metasomatized by subduction-related fluids, whose partial melting generated magmas that subsequently evolved through fractional crystallization and crustal contamination. Rare earth element (REE) patterns provide additional constraints. The syenogranites display Eu* values between 0.92 and 1.06, indicating the absence of a significant europium anomaly and limited plagioclase fractionation during crystallization. In contrast, the gabbronorites, with Eu* values ranging from 0.73 to 0.92, show a moderate negative Eu anomaly, which may reflect plagioclase depletion in the source or early fractionation of this mineral phase [58]. Although some features may appear contradictory, an integrated assessment suggests that the syenogranites originated from an enriched mantle source that experienced partial crustal contamination, as evidenced by enrichment in Cs, Ba, K, Ti, and Tm and by pronounced light rare earth element (LREE) enrichment relative to heavy rare earth elements (HREE) [20, 40]. Furthermore, elevated Rb/Sr ratios and exceptionally high Sr/Y values in some samples indicate a significant crustal contribution or localized adakitic magmatism [15, 41]. Overall, the most plausible scenario involves magma generation in a Pan-African geodynamic setting transitional between an active continental arc and a syn- to post-collisional environment [52], involving a subduction-metasomatized mantle and strong interaction with the continental crust. This interaction accounts for both mantle- and crust-derived signatures, while also explaining local variations related to internal magmatic processes.

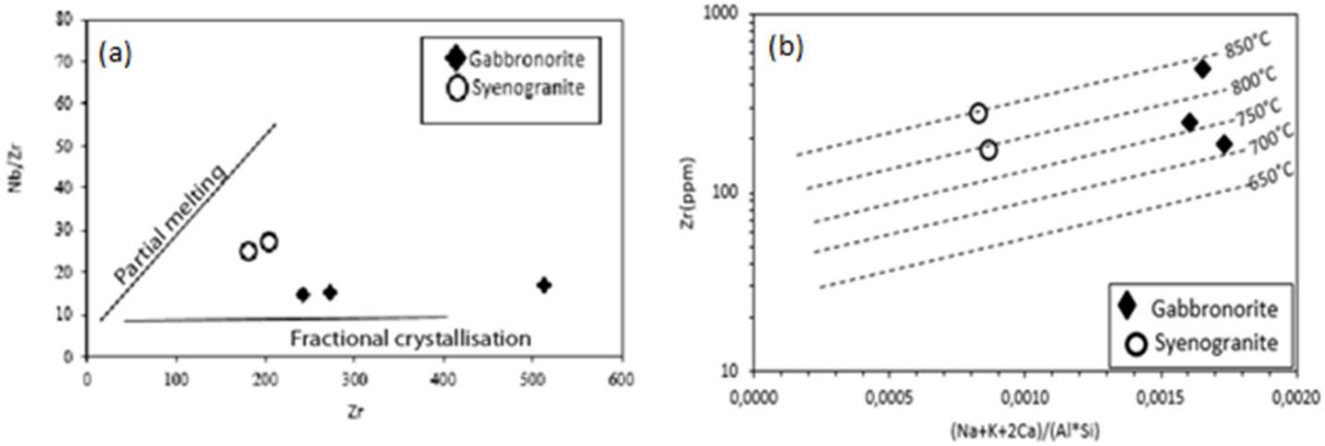

Figure 11. *(a) Nb/Zr vs. Zr diagram [3]; (b) Thermal conditions of magma emplacement, showing estimated zircon saturation temperatures [56, 8].*

5.3. Magmatic Processes and Thermodynamic Conditions of Emplacement

The Nb/Zr vs. Zr diagram (Figure 11a) allows discrimination between partial melting and fractional crystallization processes based on the contrasting behavior of two moderately incompatible elements. In the study area, the gabbronorites plot within the fractional crystallization field, displaying moderate to high Zr contents (241–513 ppm) and relatively low Nb/Zr ratios (<20). These features suggest magmatic evolution through progressive fractionation from a mantle-derived basaltic magma, possibly affected by contamination during ascent or crustal residence [40, 43]. In contrast, the syenogranites plot near the boundary between partial melting and fractional crystallization fields, with slightly higher Nb/Zr ratios and lower Zr contents. This distribution supports a crustal origin through partial melting of metasomatized or previously differentiated materials, possibly triggered by the injection of hot mafic magmas [49].

The overall dispersion of data points reflects a polyphase magmatic evolution involving both differentiated fractional crystallization and multiple partial melting events [3, 34]. The Zr versus (Na + K + 2Ca)/(Al × Si) diagram [3, 56] is used to estimate the thermal conditions of magma emplacement based on zircon saturation temperatures. According to this diagram, both syenogranite and gabbronorite magmas were emplaced at temperatures ranging between approximately 700°C and 850°C (Figure 11b).

5.4. Geotectonic Context

Granitoids are excellent indicators of tectonic evolution, particularly in subduction and collisional settings. According to Taylor and McLennan [49], granitoids formed in arc environments are enriched in Ba, Th, and U, and depleted in Nb, Sr, Ti, and P, reflecting magmas influenced by metasomatizing fluids and thickened crust. Within the Pan-African context of Cameroon, several studies [33, 37, 38, 50] attribute the emplacement of granitoids to a continental collision between the Congo Craton and the Adamawa-Yadé block. This collision would have caused crustal thickening and partial melting of the lower crust, leading to the emplacement of granitoids between 570 and 640 Ma. Ta vs. Yb and Rb vs. (Yb + Ta) diagrams ([40]; Figure 12) allow discrimination of different tectonic settings. In the study area, these diagrams indicate that all rock units were emplaced in an arc magmatic (subduction) context, with a possible transition toward a collisional (syn-collisional) environment. This suggests that the study area was situated at an active continental margin during the emplacement of these rocks [39], likely influenced by subduction processes [16]. According to Shellnutt et al. [44, 45], rocks of the Guéra Massif formed during the collision between the Congo–São Francisco Craton and the Sahara Metacraton, with active magmatism spanning approximately 50 Ma (594–545 Ma). Granites were emplaced in a collisional to post-collisional setting, displaying diverse geochemical characteristics consistent with the magmatic evolution observed in the study area.

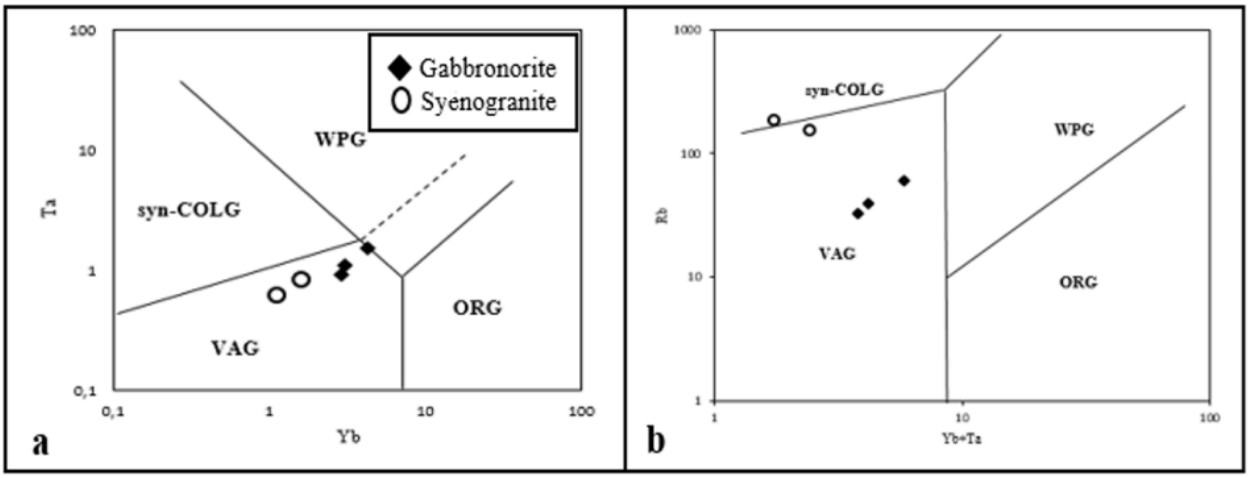

Figure 12. Tectonic discrimination diagrams after Pearce et al. [40]: (a) Ta (ppm) vs. Yb (ppm); (b) Rb (ppm) vs. (Yb + Ta) (ppm). WPG = within-plate granites; VAG = volcanic arc granites; syn-COLG = syn-collisional granites; ORG = ocean ridge granites.

6. Conclusion

The petrographic and geochemical study of syenogranites and gabbronorites from the Niergui area provides new insights into the nature, origin, and magmatic processes of the Pan-African basement in Chad. The syenogranites are strongly potassic calc-alkaline, weakly peraluminous, and ferroan, whereas the gabbronorites are metaluminous and moderately differentiated. Ma-

jor, trace, and rare-earth element geochemistry indicates a progressive magmatic evolution from a basal mantle-derived magma toward more differentiated crustal magmas, reflecting mantle–crust interaction in a bimodal setting. Isotopic and geochemical signatures, particularly Sr/Y and Rb/Sr ratios and Eu anomalies, suggest that the syenogranites originated from a mixture of enriched mantle sources and crustal contributions, while the gabbronorites record a more primitive, weakly differentiated origin. Estimated thermodynamic emplacement conditions (700–850°C) and tectonic diagrams support a subduction setting followed by a syn- to post-collisional phase, consistent with the Pan-African dynamics along the southern margin of the Sahara Metacraton. Overall, this study demonstrates that the Niergui Massif exemplifies the complexity of Pan-African geodynamics, where mantle–crust interaction, partial melting, and magmatic fractionation played a key role in the formation of the basement. These results provide a robust framework for understanding the tectono-magmatic evolution of the Guéra region and pave the way for further investigations of the Sahara Metacraton.

Author Contributions

Guoldji Crepin Djamous: Conceptualization, Data curation, Formal Analysis, Investigation, Methodology, Resources, Visualization, Writing – original draft

Tassongwa Bernard: Conceptualization, Investigation, Methodology, Project administration, Resources, Supervision, Validation, Visualization, Writing – original draft, Writing – review & editing

Metang Victor: Conceptualization, Investigation, Project administration, Validation, Visualization, Writing – original draft, Writing – review & editing

Ngassam-Mbianya Ghislain: Conceptualization, Data curation, Formal Analysis, Methodology, Resources, Validation, Visualization, Writing – original draft

Tamen Jules: Conceptualization, Data curation, Formal analysis, Methodology, Resources, Validation, Visualization, Writing – original draft

Baïssemia Ronang Gustave: Investigation, Resources, Visualization, Writing – original draft

Jouanang Viclair Daina: Investigation, Resources, Visualization, Writing – original draft

Masonde Kouo Adelaïde Flore: Investigation, Resources, Writing – original draft

Bikaga Clarisse Rosine: Investigation, Resources, Writing – original draft

Nkoumbou Charles: Conceptualization, Project administration, Supervision

Funding

This research did not receive any specific grant from funding agencies in the public, commercial, or not-for-profit sectors.

Conflicts of Interest

The authors declare that they have no known competing financial interests or personal relationships that could have appeared to influence the work reported in this paper.

References

[1] Abdelsalam, M. G., Gao, S. S., Liégeois, J. P., 2011. Upper Mantle Structure of the Saharan Metacraton. Journal of African Earth Sciences 60, 328-336.

[2] Abdelsalam, M. G., Liégeois, J. P., Stern, R. J., 2002. The Saharan Metacraton. Journal of African Earth Sciences 34, 119-136.

[3] Allegre, C. J., Minster, J. F., 1978. Quantitative models of trace element behavior in magmatic processes. Earth and Planetary Science Letters 38, 1–25.

[4] Assadi, A. O., Emmanuel, N. N., Fadimatou, Y. N. 2022. Petrogenesis and Tectonic Setting of the Gold-Bearing Magmatic Rocks of the North-Western Melfi Massif, Central Chad. European Journal of Environment and Earth Sciences 3, 23-31. https//doi.org/10.24018/ejgeo.2022.3.4.304

[5] Barbarin, B., 1999. A review of the relationships between granitoid types, their origins and their geodynamic environments. Lithos 46, 605-626.

[6] Black, R., 1980. Precambrian of West Africa. Episodes 4, 3-8.

[7] Brackman, A. J., Schwartz, J. J., 2022. The formation of high-Sr/Y plutons in cordilleran-arc crust by crystal accumulation and melt loss. Geosphere 18, 370-393. https//doi.org/10.1130/GES02400.1

[8] Boehnke, P., Watson, E. B., Trail, D., Harrison, T. M. and Schmitt, A. K., 2013. Zircon saturation Re-revisited. Chemical Geology 351, 324-334. https//doi.org/10.1016/j.chemgeo.2013.05.028

[9] Castillo, P. R., 2006. An overview of adakite petrogenesis. Chinese Science Bulletin 51, 257–268.

[10] Chiaradia, M., 2015. Crustal thickness control on Sr/Y signatures of recent arc magmas: an Earth scale perspective Sci. Rep 5, 8115.

[11] Collins, W. J., 1998. Evaluation of petrogenetic models for Lachlan Fold Belt granitoids: implications for crustal architecture and tectonic models. Australian Journal of Earth Sciences 45, 483-500. https//doi.org/10.1080/0812009980872806

[12] De La Roche, H., Leterrier, J., Grandclaude, P. and Marchal, M., 1980. A Classification of Volcanic and Plutonic Rocks Using R1R2-Diagram and Major Element Analyses—Its Relationships with Current Nomenclature. Chemical Geology 29, 183-210.

[13] Debon, F., Lefort, P., 1988. A Cationic Classification of Common Plutonic Rocks and Their Magmatic Associations: Principles, Method, Applications. Bulletin de Mineralogie 111, 493-510.

[14] Debon, F., Lemmet, M., 1999. Evolution of Mg/Fe Ratios in Late Variscan Plutonic Rocks from the External Crystalline Massifs of the Alps (France, Italy, Switzerland). J*ournal of* Petrology 40, 1151–1185.

[15] Defant, M. J., Drummond, M. S., 1990. Derivation of some modern arc magmas by melting of young subducted lithosphere. Nature 347, 662–665.

[16] Diontar, M., Kwékam, M., Fozing, E. M., Kagou, D. A., Tcheumenak, K. J., 2020. Petrology and geochemical characteristic of granitoids from Guéra massif in the central part of chad: an example of mixing magmas. Earth Science Research 9, 1927-0542.

[17] Doumnang, J. C., 2006. Géologie des formations néoprotérozoïques du Mayo Kebbi (sud-ouest du Tchad): Apports de la pétrologie et de la géochimie, implications sur la géodynamique au Panafricain. [Geology of the Neoprotezoic formations of Mayo Kebbi (South West, Chad): contribution of petrology and geochemistry, implications on the geodynamic during Pan-African]. Thèse de Doctorat, Université d'Orleans, 223 p.

[18] Ferré, E., Gleizes, G., Caby, R., 2002. Obliquely convergent tectonics and granite emplacement in the Trans-Saharan belt of Eastern Nigeria: a synthesis. Precambrian Research 114, 199-219.

[19] Freydenberg, M., 1908. Le Tchad et le bassin du Chari. These, Paris, 187 pp.

[20] Frost, B. R., Barnes, C. G., Collins. W. J., Arculus, R. J., Ellis, D. J. and Frost, C. D., 2001. A Geochemical Classification for Granitic Rocks. Journal of Petrology 42, 2033-2048.

[21] Gray, C. M., Kemp, A. I. S., 2009. The two-component model for the genesis of granitic rocks in the metasedimentary-derived and basaltic end members. Lithos 111, 113-124.

[22] Irvine, T. N., Baragar, W. R. A., 1971. A Guide to the Chemical Classification of the Common Volcanic Rocks. Canadian Journal of Earth Science 8, 523-548.

[23] Isseini, M., Andre-Mayer, A. S., Vanderhaeghe, O. Barbey, P., Deloule, E., 2012. A- Type granites from the Pan-African orogenic belt in southwestern Chad constrained using geochemistry, Sr-Nd isotopes and U-Pb geochronology. Lithos 153, 39-52.

[24] Isseini, M., Hamit, A., Abderamane, M., 2013. The tectonic and geologic framework of the Mongo area, a segment of the Pan-African Guera Massif in Central Chad: evidences from field observations and remote sensing. Revue Scientifique du TCHAD 1, 4-12.

[25] Kasser, M. Y., 1995. Evolution précambrienne de la région du Mayo Kebbi (Tchad). Un segment de la Chaîne Panafricaine. [Precambrian evolution of Mayo Kebbi (Chad): a segment of the Panafrican Belt.] Thèse de Doctorat, Muséum d'Histoire. Naturelle de Paris (France), 217 pp.

[26] Kennedy, W. Q., 1964. The structural differentiation of Africa in the Pan-African (±500 my) Tectonic episode. Annual Reports of the Institute of African Geology. 8. Leeds University, 48–49.

[27] Lacroix, A., 1925. La série lithologique de Melfi (Chari). [The lithological serie of Melfi (Chari)]. Bulletin of Geological Society of France. Paris 4th serie T XXV P. 495-500.

[28] Le Maitre, R. W., 1976. The chemical variability of some common igneous rocks. Journal of petrology. 17, 589-637.

[29] Le Maitre, R. W., Bateman, P., Dudek, A., Keller, J., Lameyre Le Bas, M. J., Sabine, P. A., Schmid, R., Sorensen, H., Streckeisen, A., Woolley, A. R., Zanettin, B., 1989. A Classification of Igneous Rocks and Glossary of Terms. Blackwell, Oxford.

[30] Liégeois, J. P., Abdelsalam, M. G., Ennih, N., Ouabadi, A., 2013. Metacraton: nature, genesis and behavior. Gondwana Research 23, 220-237.

[31] Maniar, P. D., Piccoli, P. M., 1989. Tectonic Discrimination of Granitoids. Geological Society of America Bulletin 101, 635-643.

[32] McDonough, W. F., Sun, S. S., 1995. The composition of earth. Chemical Geology 120, 223-253.

[33] Metang, V., Tassongwa B., Ngo Belnoun, Rose., Kenzo, H. A, Tawo T. M., Mbakam, K. M. D., Kengne, T. L. G., Tchop, J. L., Mouafo, L, Tchouankoue, J. P., 2022. Petrography and geochemistry of metasedimentary rocks from the southwestern portion of the Yaoundé group in Cameroon: provenance and tectonic implications. Earth Sciences 11, 232-249. https//doi.org/10.11648/j.earth.20221105.11

[34] Minster, J. F., Allègre, C. J., 1978. Systematic use of trace elements in igneous processes. Contr. Mineral. and Petrol. 68, 37–52.

[35] Ngako, V., Affaton, P., Nnange, J. M., Njanko, T. h., 2003. Pan-African tectonic evolution in central and southern Cameroon: transpression and transtension during sinistral shear movement. Journal of African Earth Sciences 36, 207–214.

[36] Nkouandou, O. F., Bardintzeff, J-M., Mahamat, O., Mefire, A. F., Ganwa, A. A., 2017. The dolerite dyke swarm of Mongo, Guéra Massif (Chad, Central Africa): Geological setting, petrography and geochemistry. Open Geosciences 9, 138-150.

[37] Nkoumbou, C., Barbey, P., Yonta-Ngouné, C., Paquette, J. L., Villiéras, D. F., 2014. Pre-collisional geodynamic context of the southern margin of the Pan-African fold belt in Cameroon. Journal of African Earth Sciences 99: 245-260.

[38] Nzenti, J. P., Abaga, B., Suh, C. E., Nzolang, C., 2011. Petrogenesis of Peraluminous Magmas from the Akum-Bamenda Massif, Pan-African Fold Belt, Cameroon," International Geology Review 53, 1121-1149.

[39] Pearce, J. A., 1983. Role of the sub-continental lithosphere in magma genesis at active continental margins. In: Hawkesworth, C. J., & Norry, M. J. (Eds.), Continental Basalts and Mantle Xenoliths. Shiva, Nantwich, pp 230–249.

[40] Pearce, J. A., Harris, N. B. W., Tindle, A. G., 1984. Trace element discrimination diagrams for the tectonic interpretation of granitic rocks. Journal of Petrology 25, 956-983.

[41] Penaye, J., Kröner, A., Toteu, S. F., Van Schmus, W. R., Doumnang, J. C., 2006. Evolution of the Mayo Kebbi region as revealed by zircon dating: An early (ca. 740 Ma) Pan-African magmatic arc in southwestern Chad. Journal of African Earth Sciences 44, 530-542.

[42] Petford, N., Atherton, M. P., 1996. Na-rich partial melts from newly underplated basaltic crust: The Cordillera Blanca Batholith, Peru. Journal of Petrology 37, 1491–1521.

[43] Rollinson, H. R., 1993. Using geochemical data: Evaluation, presentation, interpretation. Longman Scientific and Technical, Wiley, New York, 352.

[44] Shellnutt, J. G., Pham, N. H. T., Denyszyn, S. W., Yeh, M. W., Lee, T. Y., 2017. Timing of collisional and post-collisional Pan-African Orogeny silicic magmatism in south-central Chad. Precambrian Research 301, 113-123.

[45] Shellnutt, J. G., Pham, N. H. T., Yeh, M. W., Lee, T. Y., 2020. Two series of Ediacaran collision-related granites in the Guéra Massif, South-Central Chad: Tectonomagmatic constraints on the terminal collision of the eastern Central African Orogenic Belt. Precambrian Research 347, 105823.

[46] Streckeisen, A. L., 1976. Classification and Nomenclature of Igneous Rocks. N. Jahrb. Miner. Abh 107, 144-240.

[47] Streckeisen, A. L., Le Maitre, RW., 1979. A Chemical Approximation to the ModalQAPF Classification of the Igneous Rocks. Neues Jahrbuch fur Mineralogie, Abhandlungen 136, 169-206.

[48] Tarney, J., Jones, C. E., 1994. Trace element geochemistry of orogenic igneous rocks and crustal growth models. Journal of the Geological Society 151, 855-868.

[49] Taylor, S. R., McLennan, S. M., 1985. The Continental Crust: Its Composition and Evolution. Blackwell Scientific, Oxford.

[50] Tchakounté, J. N., Fuh, C. G., Kamwa, A. N., Metang, V., Mvondo, O. J., Nkoumbou, C., 2021. Petrology and geochemistry of the Pan-African high-K calc-alkaline to shoshonitic - adakitic Bapé plutonic suites (Adamawa-Yade block, Cameroon): evidence of a hot oceanic crust subduction. International Journal and Earth Sciences 110, 2067 - 2090.

[51] Tchameni, R., Pouclet, A., Penaye, J., Ganwa, A. A., Toteu, S. F., 2006. Petrography and Geochemistry of the Ngaoundere Pan-African Granitoids in Central Cameroon: Implications for Their Sources and Geological Setting. Journal of African Earth Sciences 44, 511-529.

[52] Toteu, S. F., Penaye, J., Poudjom Djomani, Y. H., 2004. Geodynamic evolution of the Pan African belt in Central Africa with special reference to Cameroon. Canadian Journal of Earth Sciences 41, 73–85.

[53] Trompette, R., 2000. Gondwana Evolution; Its Assembly at Around 600 Ma. Earth and Planetary Science 330, 305-315.

[54] Vincent, P., 1954. Coupure An Timan Ouest. Rapport de fin de mission 1953 – 54. D. M. G. Brazzaville.

[55] Vincent, P. M., 1956. Extraction du zircon dans un granite intrusif porphyroïde en provenance du District de Melfi n° R6-4 (coupure géologique d'AmTiman-ouest). [Zircon extraction in an intrusive porphyroid granite from Melfi District n° R6-4 (geological map of western AmTiman). Brazzaville, Direction des Mines et de la Géologie.

[56] Watson, E. B., Harrison, T. M., 1983. Zircon saturation revisited temperature and composition effects in a variety of crustal magma types. Earth and Planetary Science Letters 64, 295-304.

[57] Wedepohl, K. H., 1995. The Composition of the Continental Crust. Geochimica et Cosmochimica Acta 59, 1217-1232.

[58] Wilson, M., 2007. Igneous Petrogenesis: A Global Tectonic Approach. Springer, p 466.

[59] Wolff, J. P., 1964. Carte géologique de la République du Tchad au 1:1 500 000. [Geological map of Chad Republic of 1:1 500 000 scale]. Bureau de Recherches Géologiques et Minières (BRGM), Paris.